ELSEVIER

# An alternative approach for recording of multidimensional NMR data based on frequency dependent folding mechanism

Peyman Sakhaii [a,1], Burkhard Haase [a,1], Wolfgang Bermel [b,*]

[a] *Sanofi-Aventis Deutschland GmbH, Process Development Chemistry, PDC SPS (Structure Elucidation/Project & Production Support),
Industriepark Hoechst, Building G 838, Labor 204, D-65926 Frankfurt/Main, Germany*
[b] *Bruker BioSpin GmbH, Silberstreifen, D-76287 Rheinstetten, Germany*

This work is dedicated to associate Prof. Takahisa Ikegami.

## Abstract

A new scheme for obtaining HSQC spectra with improved resolution or in a shorter time called SHARC (Shaped Arrayed data aCquisition protocol) is proposed, which uses region selective RF pulses and allows the sweep width to be adjusted individually for each region. It thus bypasses the problems with the Nyquist theorem associated with other method suggested for this purpose. Assignment of the cross-peaks to their respective region is achieved by manipulating the phases of the RF pulses and/or their frequencies. SHARC NMR can be applied without any previous knowledge of the chemical shift distribution, but can be further optimized on the basis of a quick overview spectrum.
© 2008 Elsevier Inc. All rights reserved.

## 1. Introduction

Ever since its introduction multidimensional NMR spectroscopy is providing an astonishingly versatile concept for enhancing the capabilities of NMR [1–3]. In the past, long measurement times were required to improve the signal-to-noise ratio in NMR spectra, and to obtain sufficient spectral resolution in the indirectly detected dimensions of multidimensional NMR data. More recently the number of situations has increased, where a high demand for significant shortening of the experimental time is desirable. In the literature two different scenarios considering time limitations of any NMR acquisition are described. These are often referred to as sensitivity-limited and sampling-limited regimes. In the first case the amount of available sample is limited, leading to an increased number of scans and thus prolonged measurement time to obtain the required signal-to-noise ratio. In the sampling or resolution limited regime the total measurement time is rather dominated by the digital resolution reflected in the number of acquired data points in $t_1$. It can be assumed that in the sampling-limited regime the prevailing signal-to-noise ratio of the spectrum is more than sufficient. Recently, the sampling-limited regime has received significant attention and is addressed by several fast acquisition methods. A broad range of technical approaches has hitherto been propagated.

A first class of methods allows reducing the number of acquired data points in the indirect dimension. Examples are reduced dimensionality [4–6] or projection NMR [7–9], Hadamard type [10–13] or spatially encoded frequency labeling [14–16] and non-linear time domain sampling, combined with appropriate data processing algorithms

[17–19]. A second class of recently proposed methods to reduce the acquisition time is based on shortening the delay between consecutive scans to achieve higher repetition rates. Proton relaxation optimization techniques in combination with an Ernst-angle excitation scheme ensure optimum sensitivity for short recycle delays. Both are jointly contributing to a higher $S/N$ per unit time [20–22]. A Cogwheel phase cycling has been proposed as an alternative approach to the conventional nested phase cycling protocol. Whereby, in some examples, a considerable reduction in the number of phase cycling steps, required for the selection of requested coherence levels has been illustrated [23]. A computerized grid search with respect to the coherence transfer pathway diagram must be applied to find the appropriate phase cycling scheme. Examples were given both in Solid State [24] and Liquid State NMR [25]. Covariance NMR spectroscopy has been shown to provide maximal resolution along multiple frequency axis [26]. The scheme yields correlation spectra with high spectral resolution from small data sets. About a decade ago, a proof of concept was provided to run several multidimensional NMR experiments by simultaneous acquisition of $^{13}C$ and $^{15}N$ HSQC [27,28]. Recently, it was reported that several multidimensional NMR spectra of different nuclear species could be acquired by a parallel acquisition approach (PANSY) [29]. For this the probehead must have the capability to be tuned to different nuclei independently and in addition the system has to be equipped with a separate receiver for each nuclear species that is to be detected.

A different way of reducing the acquisition time is the application of spectral aliasing [30–32]. Normally, multidimensional NMR spectroscopy must satisfy the Nyquist sampling theorem $\Delta t_{1,\text{Nyq}} = 1/(\text{spectral width})$ [33] for correct digitization in all frequency dimensions. Therefore, if we require fine digital resolution in the $F_1$ dimension and if the spectrum covers a wide frequency range, the two-dimensional experiment must employ a large number of $t_1$ increments. This requires long experiments and large data arrays. A simple way out of this dilemma is just reducing the sweep width in the indirect dimension. Basically, standard pulse sequences are used to acquire several spectra with different reduced spectral widths in the indirect dimensions. Rules have been deduced for the selection of the reduced sweep width so that the correct chemical shifts in $t_1$ can be reconstructed. The measurement time is saved by reducing the number of $t_1$ increments [34,35].

A novel approach is submitted here that bypasses the sampling restrictions associated with the Nyquist theorem constraints. The developed framework is making intensive use of a suite of frequency selective RF pulses in close combination with storage of magnetization along the $z$-axis. Very recently, we introduced a novel *frequency dependent folding* theorem [36]. In this paper, we would like to give a short introduction into the basics and technical implementation of the SHARC technique (*Sh*aped *Ar*rayed data a*C*quisition protocol). From now on, our discussion is elaborated on the basis of an elementary HSQC pulse sequence with its associated product operators [37].

## 2. Results and discussion

For the majority of HSQC-based NMR experiments there is a simple correlation between heteronuclear frequency and indirect domain spectral width. Fig. 1 is demonstrating the standard situation, where a heteronuclear frequency bandwidth of 100 ppm is correlated to a given value of indirect domain spectral width. The value of the indirect domain spectral width $sw_1$ is directly given by the Nyquist theorem constraint as input for correct digitization of the chemical shift. The optimum magnitude of the indirect domain spectral width is determined by the size of the selected bandwidth itself and is set to be 100 ppm. According to Fig. 1 if we decrease the indirect domain spectral width lower than the value given by the Nyquist theorem (100 ppm) the cross-peaks outside of the indirect domain spectral width will be folded. In contrast, if we increase the indirect domain spectral width higher than the value given by the Nyquist theorem we may lose digital resolution but do not observe any folding of cross-peaks.

This assumption that hitherto linked *broad band* heteronuclear frequencies with a single value of indirect domain spectral width is abandoned in this work. The graphs shown in Figs 2a and b are describing two scenarios of relations between heteronuclear frequencies and indirect domain spectral width. The graph in Fig. 2a is representing a class of experiments, where three predefined heteronuclear frequency regions are correlated with three different values of indirect domain spectral width. The optimum size of each individual indirect domain spectral width is taken from the graphs shown in Figs. 2a and b. The size of $sw_1$
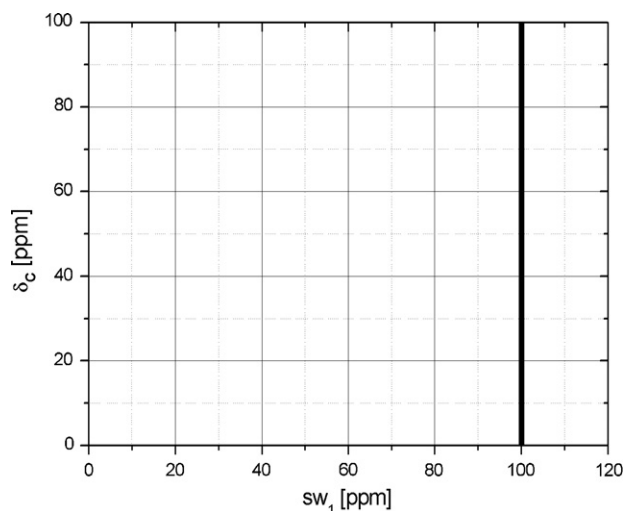


Fig. 1. The graph is illustrating how a heteronuclear frequency bandwidth of 100 ppm is correlated to its optimum size of the indirect domain spectral width of 100 ppm. The $y$-axis represents the broad band $^{13}C$ chemical shift range. The $x$-axis displays the size of the indirect domain spectral width in $t_1$.
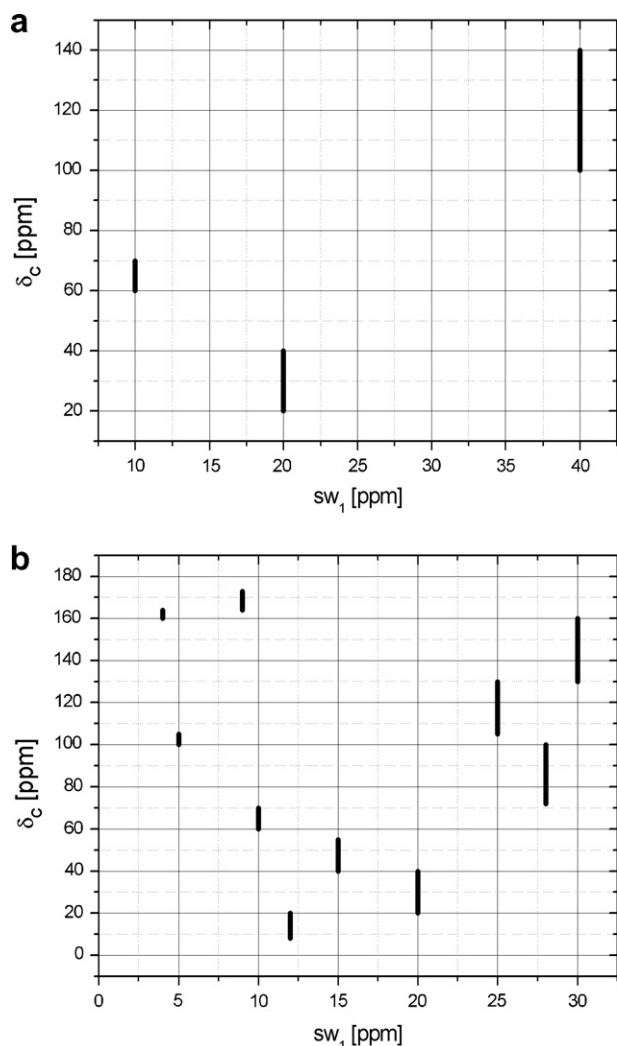
Fig. 2. (a) The graph is illustrating how three different spectral ranges (from 60 to 70 ppm with an optimum $sw_1$ of 10 ppm; from 20 to 40 ppm with an optimum $sw_1$ of 20 ppm and finally from 100 to 140 ppm with an optimum $sw_1$ of 40 ppm) are correlated to the optimum sizes of their indirect domain spectral widths ($sw_1$). The size of each individual $sw_1$ is displayed in true scale and is further matched to Nyquist condition. (b) The graph is demonstrating how 10 different spectral bandwidths are associated to the optimum sizes of their indirect domain spectral widths. The size of each individual $sw_1$ is displayed in true scale and is further matched to Nyquist condition.

is displayed in true scale and is further matched to Nyquist condition. This class of acquisition arrangement can be easily generalized and extended to provide an arbitrary number of heteronuclear frequency regions with any desired value of indirect domain spectral width. The graph in Fig. 2b is describing an experiment, where a number of 10 heteronuclear frequency regions were correlated with respective values of the indirect domain spectral widths.

The difference between the "*normal*" folding achievable just by simply reducing the sweep width in $t_1$ (Fig. 1) and frequency dependent folding, can be best understood by comparing the effect of a single violation of the Nyquist theorem applied to a recorded HSQC data set. In the case of normal folding the $F_1$ chemical shift values of all cross-

peaks outside of the indirect domain spectral window will be reflected at the edge of the spectrum. The entire range of heteronuclear frequencies is correlated to a single reduced indirect domain spectral width (Fig. 1). How often a signal gets reflected depends on the distance of the $F_1$ resonance frequencies from the carrier frequency of the heteronuclear channel. In contrast to the *normal* folding, the frequency dependent folding theorem opens up a new opportunity of non-uniformly assigning the sweep widths to different frequency bandwidths. In SHARC spectroscopy each individual bandwidth comprises its own carrier frequency and indirect domain spectral width ($sw_1$). This is practically realized by selective perturbation of $zz$ spin magnetization [38,39]. This issue will be further discussed in more detail by means of Figs. 1, 2a,b, 3.

Suppose we define three different chemical shift bandwidths $S_i$ from 20 to 40 ppm, $S_j$ from 60 to 70 ppm and finally $S_k$ from 100 to 140 ppm in a proton decoupled [$^{13}$C, $^1$H] heteronuclear single quantum correlation (HSQC) experiment (Fig. 3).

Now, if we apply selective excitation RF pulses to these individual frequency ranges $S_i$, $S_j$ and $S_k$ and if we allow chemical shift evolution of the antiphase $S$ magnetization $2I_zS_y$ preferably with unequal evolution delays then the two-dimensional experiment is basically enabled to provide each individual spectral range $S_i$, $S_j$ and $S_k$ with its targeted unique $F_1$ spectral window (Fig. 3). The interaction of the spectral ranges $S_i$, $S_j$ and $S_k$ with their corresponding spectral widths in $F_1$ is displayed in Fig. 2a. This graph is clearly demonstrating how each individual spectral range $S_i$, $S_j$ and $S_k$ is associated to its optimum size of indirect domain spectral width. It is important to consider that the signal folding of each individual indirect domain spectral width can be suppressed by setting the current carrier frequency at the center of each indirect domain spectral width and using the optimum size of indirect domain spectral window. The ideal value of $sw_1$ is directly determined by the magnitude of the current bandwidth.
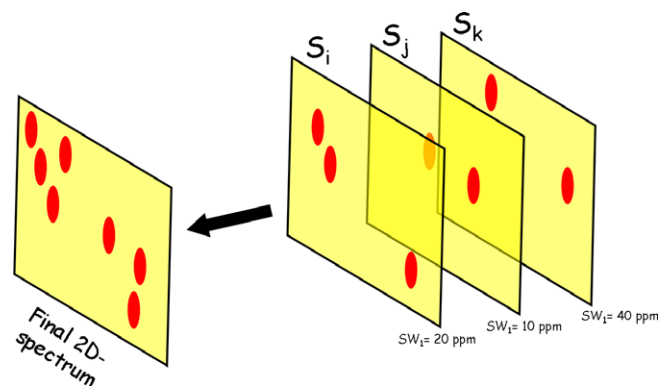


Fig. 3. Three different bandwidths ($S_i$ from 20 to 40 ppm, $S_j$ from 60 to 70 ppm and $S_k$ from 100 to 140 ppm) are associated to their indirect domain spectral width $sw_1$ of 20 ppm, 10 ppm and 40 ppm. The final 2D spectrum contains cross-peaks stemming from the individual bandwidth $S_i$, $S_j$ and $S_k$. Each individual bandwidth comprises its unique indirect domain spectral width $sw_1$.
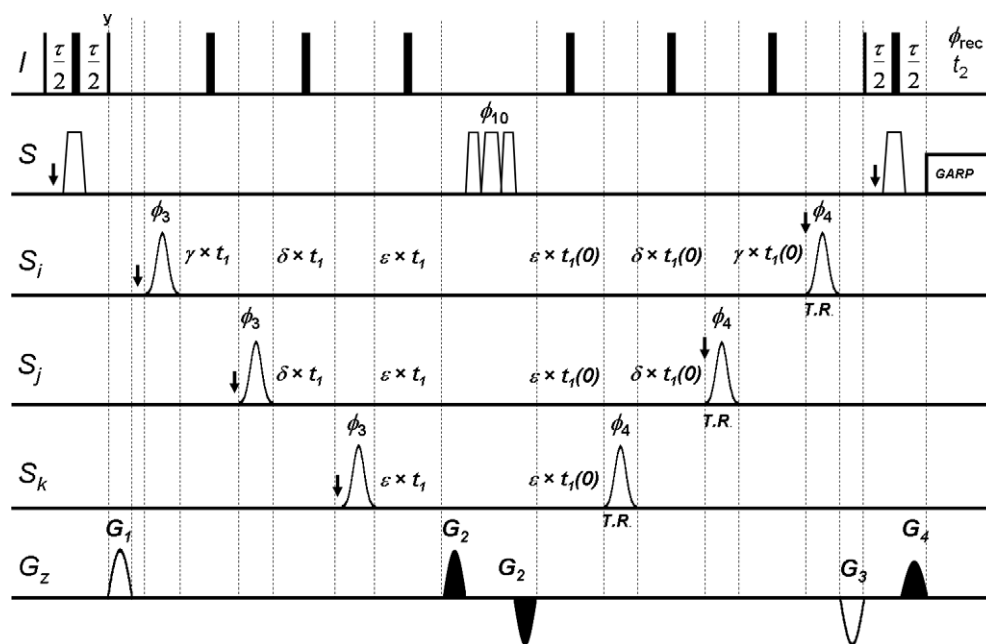
Fig. 4. Pulse sequence A was originally designed for the demonstration of frequency dependent folding mechanism and represents the first pulse sequence of a series of novel HSQC type sequences by which fundamental principles of spectral folding were evaluated. The frequency discrimination in $t_1$ is achieved by an Echo/antiEcho mode protocol. Individual assignment of frequency bandwidth to $sw_1$ is carried out in dependence of succeeding spectral windows (nested encoding scheme). A broadband composite adiabatic pulse is used as 180° refocusing pulse. With this each flipback pulse automatically compensates for Bloch–Siegert shifts [56,57]. Detailed description of pulse sequence elements and delays is given in the experimental part.

We must further discuss two major technical differences associated with these selective $t_1$ labeling techniques. The individual assignment of the frequency bandwidths $S_i$, $S_j$ and $S_k$ to their respective spectral window is optionally carried out either independently from consecutive bandwidths and thus in an arbitrary fashion (pulse sequences B and C; Figs. 5 and 6) or in full dependence of succeeding spectral windows. The latter corresponds to a nested encoding scheme (pulse sequence A, Fig. 4), where the first region to be excited is the one with the smallest bandwidth (largest increment) and the last the one with the largest bandwidth (smallest increment).

Actually, there is an underlying precept to deduce the SHARC type pulse sequences by envisioning the mode of action of frequency swept adiabatic pulses. We have to keep in mind that adiabatic pulses could theoretically be decomposed in N phase modulated shape pulses with finite duration, where the offset of irradiation is swept over a particular frequency range [40,41]. Suppose we would put evolution periods between these consecutive shape pulses, then we come up with pulse sequence constructions like Fig. 4 with synchronous incrementation of $t_1$ evolution delays. For the sake of simplicity three frequency bandwidths $S_i$, $S_j$ and $S_k$ are used throughout the text and pulse sequences A–C.

The objective fact to simultaneously expand several evolution periods is not new. Related pulse sequences were first demonstrated by Bodenhausen et al. and have found wide applications better known under the acronym ACCORDION NMR spectroscopy [42]. Interestingly,

several very novel publications highlighting RD (reduced dimensionality) or projection NMR spectroscopy [43–45] are extensively using the basics of joined evolution periods.

A pulse scheme like the one shown in Fig. 4 can only represent the starting framework of a new series of relaxation optimized pulse sequences. Therefore, we took measures first to reduce the loss in signal intensity observed by dissipative transversal relaxation processes of the magnetization being involved in the frequency selective operations. As depicted in Fig. 4 the first excited frequency bandwidth is already in transverse plane, when the next shape pulse is executed. This operational characteristic has been optimized and replaced in pulse sequences B (Fig. 5) and C (Fig. 6), where $t_1$ evolution periods are arranged one after another. This allows frequency jumps from one $t_1$ evolution period to the next and thus avoids the problem of folding in the resulting spectra.

An enhanced protocol of SHARC acquisition technique is derived by just minimizing the size of the indirect domain spectral width in order to cover the desired chemical shift distributions in the frequency space and by setting the current carrier frequency at the center of its indirect domain spectral width. These acquisition attributes have led to the development of pulse sequences B and C. The technical implementation of the frequency jumps in $F_1$ is straightforward. The architecture of pulse sequence constructions B and C is designed to take advantage of selective excitation of $zz$ spin magnetization along with its band selective $t_1$ evolution.
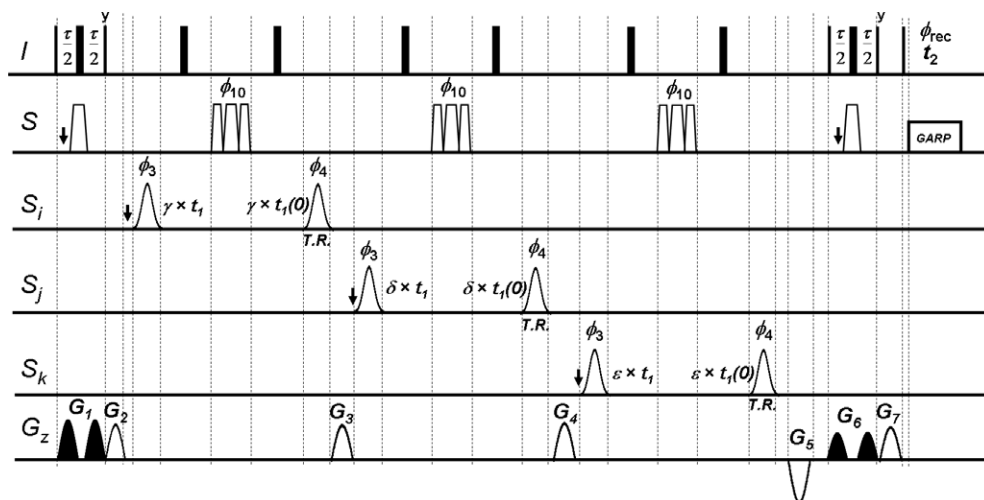
Fig. 5. The pulse sequence B represents an advanced version of frequency dependent excitation scheme. The frequency discrimination in $t_1$ is achieved by States-TPPI protocol. A loss in signal intensity due to diffusion processes caused by field gradient labeling is eliminated. Gradient strengths are randomly selected to suppress undesired magnetization. The 180° refocusing pulse in the middle of each block is shifted to act at 75 ppm by means of a linear phase ramp [58], frequency changes are indicated by vertical arrows. Detailed description of pulse sequence elements and delays is given in the experimental part.
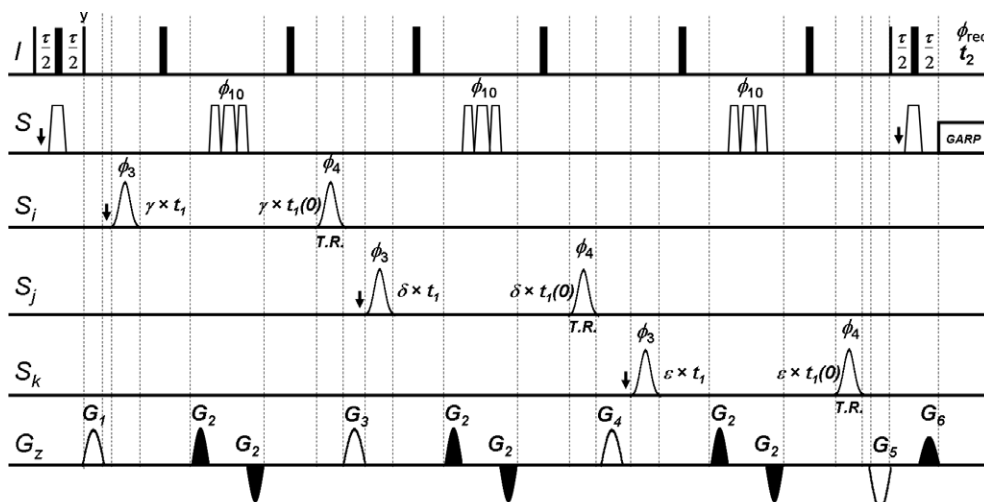


Fig. 6. The sequence C is selecting the desired coherence pathway by application of suitable gradient pulses. The bipolar gradient pulses applied in the $t_1$ evolution period are working in a bi-functional way. On the one hand the desired coherence pathways of selectively excited $2I_zS_y$ magnetization are selected, while on the other hand the same bipolar gradient pulses are concurrently acting as additional crusher filter for $2I_zS_z$ coherences. The 180° refocusing pulse in the middle of each block is shifted to act at 75 ppm by means of a linear phase ramp [58], frequency changes are indicated by vertical arrows. Detailed description of pulse sequence elements and delays is given in the experimental part.

Unperturbed $zz$ spin magnetization is invariant with respect to local $t_1$ evolution and to any carrier frequency variation. Besides relaxation losses can only occur due to $T_1$ relaxation, where the rates are smaller than for $T_2$. The execution of related pulse sequences B and C will result in a standard experimental setup and does not oblige the application of any unusual chemical shift back-calculation algorithm of the acquired NMR data. This is due to the fact, that we reduce the indirect domain spectral width to cover the desired frequency range but a violation of the Nyquist condition is always avoided.

The salient feature of the SHARC type experiments will be demonstrated by means of a regular proton decoupled

[$^{13}$C, $^{1}$H] heteronuclear single quantum correlation experiment (HSQC) pulse sequence B (Fig. 5).

For a $^{13}$C spin, $S$ at angular offset frequency $d$, coupled to its proton, $I$, antiphase $I$ spin magnetization, $2I_xS_z$ is generated at the end of the second $\tau/2$ period. The antiphase $I$ spin magnetization $2I_xS_z$ is then transferred to unobservable $2I_zS_z$ spin magnetization. This $zz$ spin magnetization is thus stored along the $z$-axis for a later recall in the HSQC sequence and is representing a pool of spin quantum information. The potential feature of $z$-filter technique has been widely used in fields of MRI [46,47], Solid State [48] and Liquid State NMR [49,50] considering the suppression of unwanted transverse magnetization by

phase cycling or pulsed field gradients. At this point of the pulse sequence B (Fig. 5), selective radiofrequency (RF) 90° pulses are applied, so that only antiphase $S$ spin magnetization, $2I_zS_y$ from the desired narrow frequency range is created. This antiphase $S$ magnetization, $2I_zS_y$ is propagated for a $t_1$ evolution period like in a regular HSQC experiment. Particular care should be given to two issues associated with the application of selective irradiation to $zz$ spin magnetization. Firstly, we have to compensate the phase evolution during the selective pulses, which depends on the type of pulses used. This is accomplished by the introduction of a non-selective carbon refocusing pulse in the midway of the evolution and compensation delay and by time reversing the second selective pulse. For the time point $t_1(0)$, these delays are set to the same value. The proposed pulse sequence element consisting of two selective excitation pulses and a non-selective refocusing pulse will refocus all initial phase evolution and is from now on designated as self compensated block of RF shaped pulses. The second shaped 90° pulse returns the antiphase $S$ magnetization $2I_zS_y$ back to the $2I_zS_z$ state. Secondly, the heteronuclear $J_{HC}$ coupling must be refocused. Non-selective proton inversion pulses are inserted in the midway of the evolution and compensation periods for this purpose. Interaction of the antiphase $S$ magnetization, $2I_zS_y$ with the self compensated block of RF shaped pulses was investigated by means of a phase evolution diagram [51] to disclose the refocusing of the heteronuclear $J_{HC}$ coupling. Now, let us continue analyzing the further destiny of $zz$ spin magnetization. The magnetization oriented in the $z$-direction is not time-modulated by chemical shift and is robust in the face of strong transverse relaxation processes and is subject only to much less severe effects of longitudinal spin–lattice relaxation. The procedure is recursive and can in principle be extended to N narrow frequency ranges in the indirect dimension. It is worth mentioning, that undesired magnetization is destroyed by randomly adjusted gradient pulses. The gradient pulses (pulse sequence B) (Fig. 5) are contrived to be executed before and after each self compensated block of RF shaped pulses. After completion of selective chemical shift evolution of the $S$ magnetization, a reverse INEPT part creates antiphase $I$ magnetization, $2I_yS_z$, which is then refocused to in-phase magnetization. At this stage of the pulse sequence B, we decided to introduce an additional z filter on $I$ magnetization, which will help the experimental setup to purge once again undesired magnetization and consequently help to maximize the receiver gain prior to detecting the signal response. A read out pulse on $I$ magnetization will finally create observable in-phase magnetization and data acquisition is being performed. Finally, the magnetization returns to a steady state with elapse of time. The quadrature detection in the $t_1$ dimension is achieved by incrementing the phases $\varphi_3$ of the 90° S spin selective pulses preceding each $t_1$ evolution period by means of States-TPPI protocol. Furthermore attention was given to the phases $\varphi_3$ of the 90° S spin selective pulses, which are being manipulated by appropriate

encoding schemes. As shown in Fig. 6 the experiment can also be performed in an Echo/antiEcho mode using gradient coherence selection.

In the following the results of the SHARC approach are illustrated using the cyclic octapeptide Hymenistatin cyclo(-Pro-Pro-Tyr-Val-Pro-Leu-Ile-Ile) as an example. Fig. 7 shows the conventional HSQC spectrum of this molecule together with four regions of 42 ppm each, which are slightly overlapping (by 2 ppm). As depicted in Fig. 3 those four regions will be superimposed in the SHARC spectrum. This can be seen in Fig. 8. Since the carrier frequency and the width for each region are known four different ppm axis can easily be calculated and plotted alongside of the spectrum. This leads to the question how the cross-peaks can be assigned to the different regions of the spectrum? There are several possible strategies. In the first one the phases $\varphi_3$ of the 90° S spin pulses are alternated between 0° and 180°. This results in a change in peak sign between adjacent regions. Since there is a vaguely linear correlation between proton and carbon chemical shifts, signals from different carbon regions may well be reasonably separated in proton chemical shift so that this approach could be sufficient in a lot of cases. In Fig. 8 the left hand region with two cross-peaks corresponds to that around 135 ppm. The region around 95 ppm does not contain any peaks. The remaining peaks are easily assigned to the regions around 55 and 15 ppm, respectively, as they differ in sign. The inserts show an expansion of a crowded region. The upper panel is from the conventional HSQC (Fig. 7), the lower from the SHARC HSQC, both recorded in the same experimental time and processed with identical parameters. It should be noted, that processing methods improving resolution like zero-filling or linear prediction are applicable to SHARC HSQC spectra the same way. The increase in resolution nicely separates the peaks and allows determining the peak position unambiguously.

In case there is overlap between individual regions the experiment can be repeated, but this time with slightly modified carrier frequencies (region 1 +0.25 ppm, region 2 −0.25 ppm, region 3 +0.5 ppm, etc.). Thus by identifying the change in the apparent peak position a peak can immediately be assigned to a particular region. The drawback is a factor of two either as increase in the overall experimental time or as loss in resolution. Fig. 9 shows two spectra acquired in this way (this time with six regions of different width, see below). Again six different ppm axes can be calculated (not shown for reason of space). The analysis of the spectrum is illustrated by showing the difference in apparent peak position for three selected cross-peaks from regions 2, 6 and 3, respectively (top to bottom), which can easily be determined. As shown both schemes (alternating peak signs and changes in peak position) can be combined in one experiment.

In rather crowded spectra, where a slight change in carrier frequency is not sufficient, there might be the need to separate different regions into subspectra. This can be achieved by again running two experiments. The first one
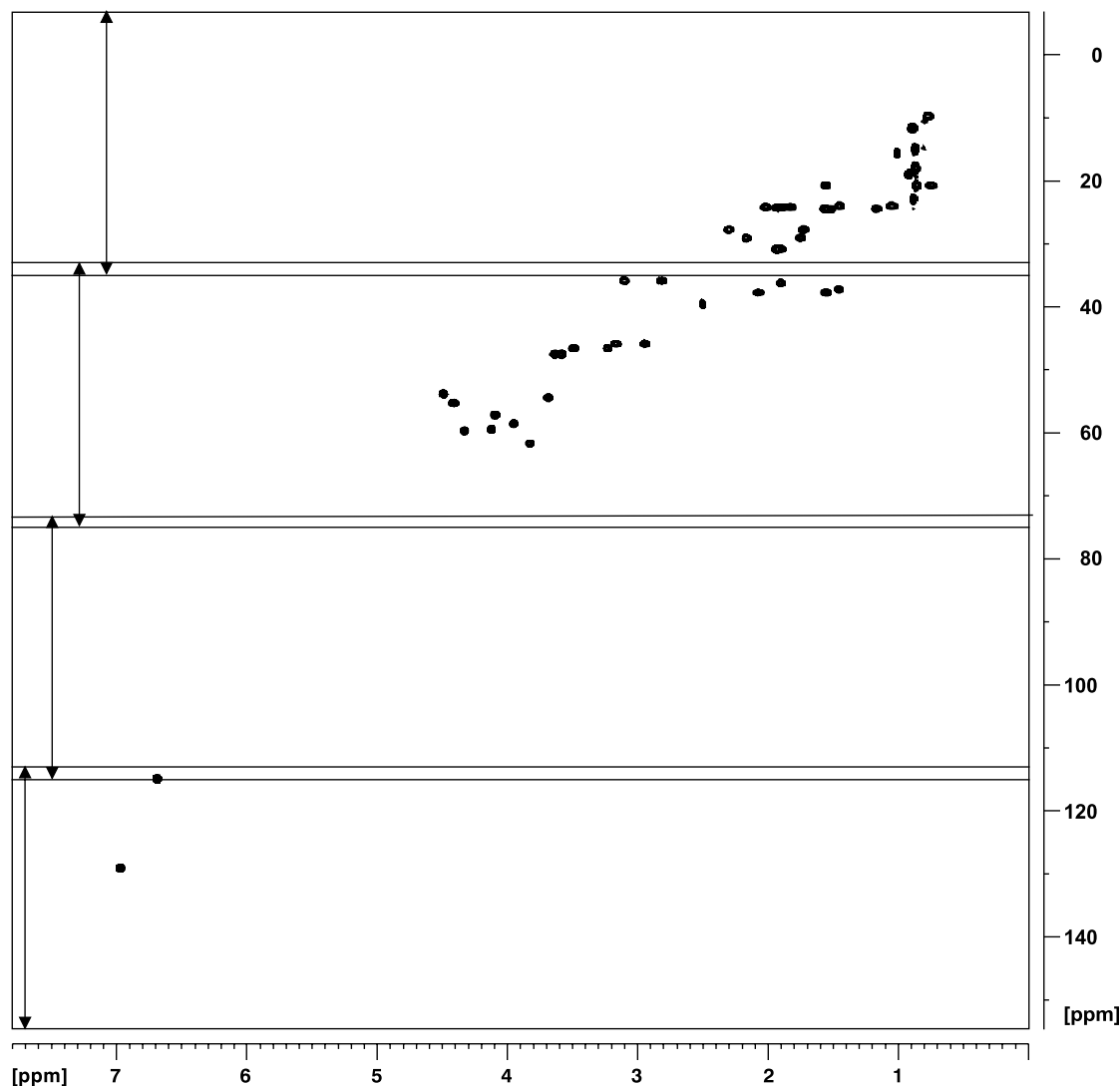
Fig. 7. 2D HSQC spectrum of Hymenistatin/DMSO-$d_6$ using a regular pulse sequence, which has, except for the conventional $t_1$ evolution period, the same features (States TPPI, spoil gradients, $z$-filter) as the SHARC HSQC sequence in Fig. 5.

is the normal SHARC HSQC. For the second the phase of the excitation pulse for half of the regions is changed by 180°, thus inverting the peaks for part of the spectrum. Calculating sum and difference between both experiments will result in two subspectra each of which shows the cross-peaks for half the total number of regions. This approach follows the same philosophy as other bandselective experiments [54], using shaped pulses which encode a Hadamard matrix, here for the simplest case of $2^n$ with $n = 1$. The result is shown in Fig. 10 where four regions are subdivided into two subspectra (region 1 and 3 versus 2 and 4). Since the peaks of the two regions within a subspectrum still have opposite signs all peaks can unambiguously be assigned to their respective regions. Since the approach requires two experiments to be run (usually in an interleaved fashion) there is, like in the previous approach, again a factor of two in increase in overall experimental time or loss in resolution. The last concept can easily be extended such that it follows Hadamard matrices of higher order ($2^n$ with

$n = 2, 3, \ldots$) Of course this will require an increasing number of experiments to be run (also $2^n$), which will be more costly for time or resolution to the extend that it may eventually void the advantages of the method. Nevertheless this way it is possible to obtain subspectra with only a single region each.

As shown in Fig. 8 a SHARC HSQC spectrum can be recorded by simply using one fourth of the sweep width for each region. For this no previous knowledge of the chemical shift distribution is required. But as it turns out one of the four regions actually does not contain any cross-peak. This region does not contribute to the spectrum but can lead to signal loss due to longitudinal spin–lattice relaxation of the $zz$ spin magnetization during unnecessary building blocks. So leaving out blank regions of the spectrum is of advantage, in particular when this can be combined with narrowing the width of the region and thus improving the resolution. When separating the peaks into different subspectra this will even be more beneficial
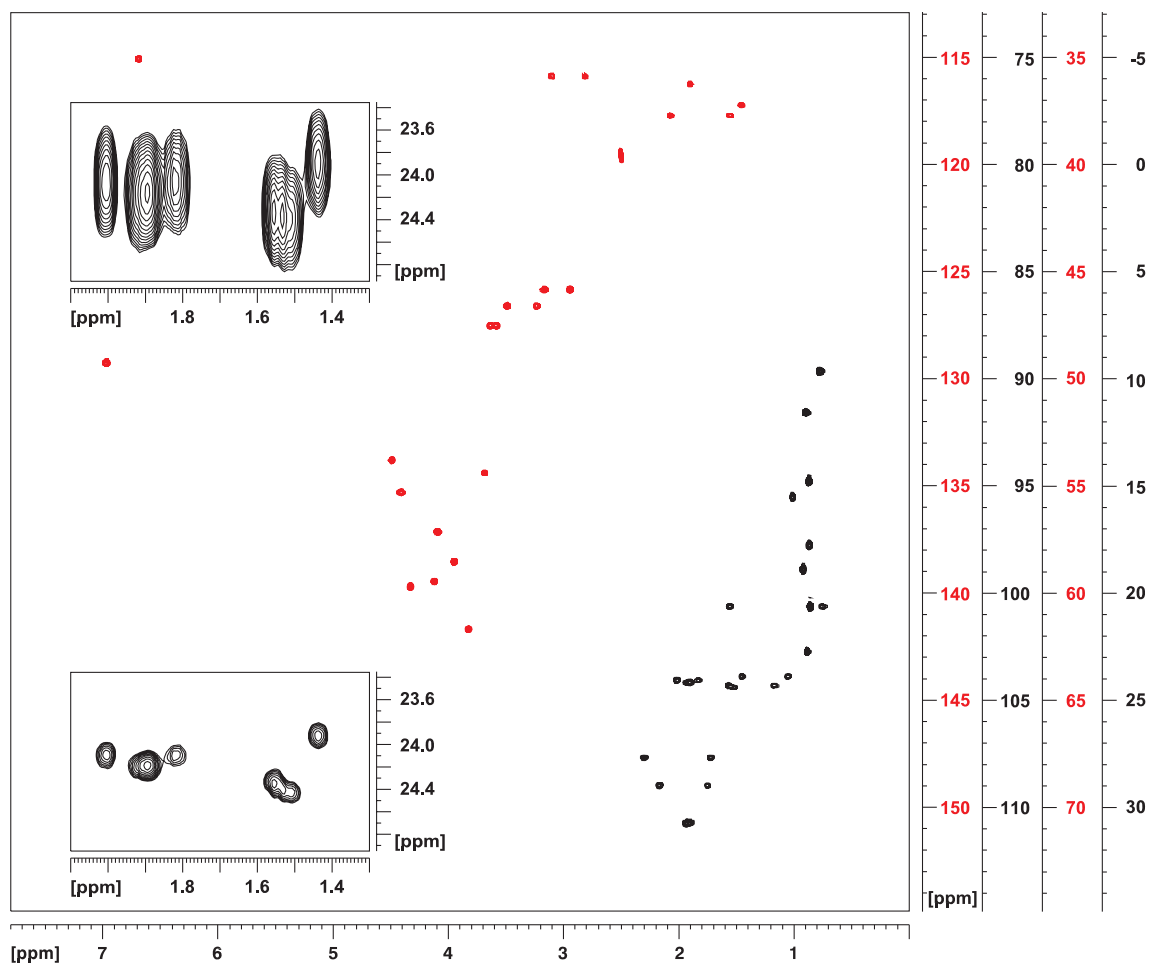
Fig. 8. 2D SHARC HSQC spectrum of Hymenistatin/DMSO-$d_6$ recorded utilizing the pulse sequence B (Fig. 5) with four regions of 42 ppm each. The sign of the peaks alternates for adjacent regions. The spectrum is shown with multiple axes for the $^{13}$C chemical shifts corresponding to the four regions. Black and red contours indicate positive and negative peaks. The color of the axes matches the color of the cross-peaks. The upper insert shows a selected part of a normal HSQC, whereas the lower one shows the same part of the SHARC HSQC.

because unnecessary additional experiment can be avoided, which reduces the experiment time. Within a given class of compounds it may be possible to obtain generic regions from known members of the class. This is illustrated in Fig. 9 where three regions of 25 ppm each have been defined between 0 and 75 ppm to cover the range of the aliphatic carbons of the peptide spectrum. A fourth region of 25 ppm was placed around 125 ppm to include the aromatic resonances. Even though two experiments have been recorded in the same experimental time as the regular HSQC to separate the data into two subspectra, thus reducing the obtained resolution by a factor of two, the comparison of the two inserts shows that narrowing the width of the regions still leads to a significant improvement in resolution.

Knowledge about the chemical shift distribution can also be obtained by running an overview spectrum. For this only a low resolution broadband HSQC is required. The chemical shift information from this low resolution spectrum is then directly encoded into the set up of the selective RF shaped pulses. The insert in Fig. 10 shows yet another

improvement in resolution compared to the previous spectra due to the fact that the width of the region is now optimized based on previous knowledge of the chemical shift distribution. The black cross-peak belongs to a different region.

How many data points in the indirect dimension are required for the low resolution spectrum? For that purpose, we analyzed the stepwise convergence of line width improvement by processing a HSQC data set while gradually increasing the number of $t_1$ data points involved in the processing scheme. According to the diagrams depicted in Figs. 11 and 12, already after about 15 complex data points the speed of line width narrowing becomes very slow (about 200 Hz at a peak width of approximately 2 kHz). Finally, the presented protocol can even be further optimized by conducting a magnitude mode preparation experiment giving a prolonged acquisition time in $t_1$. This is due to the fact that the magnitude mode preparation experiment logically abandons the quadrature detection in $t_1$ and uses the data points for a further evolution in the indirect domain acquisition time.
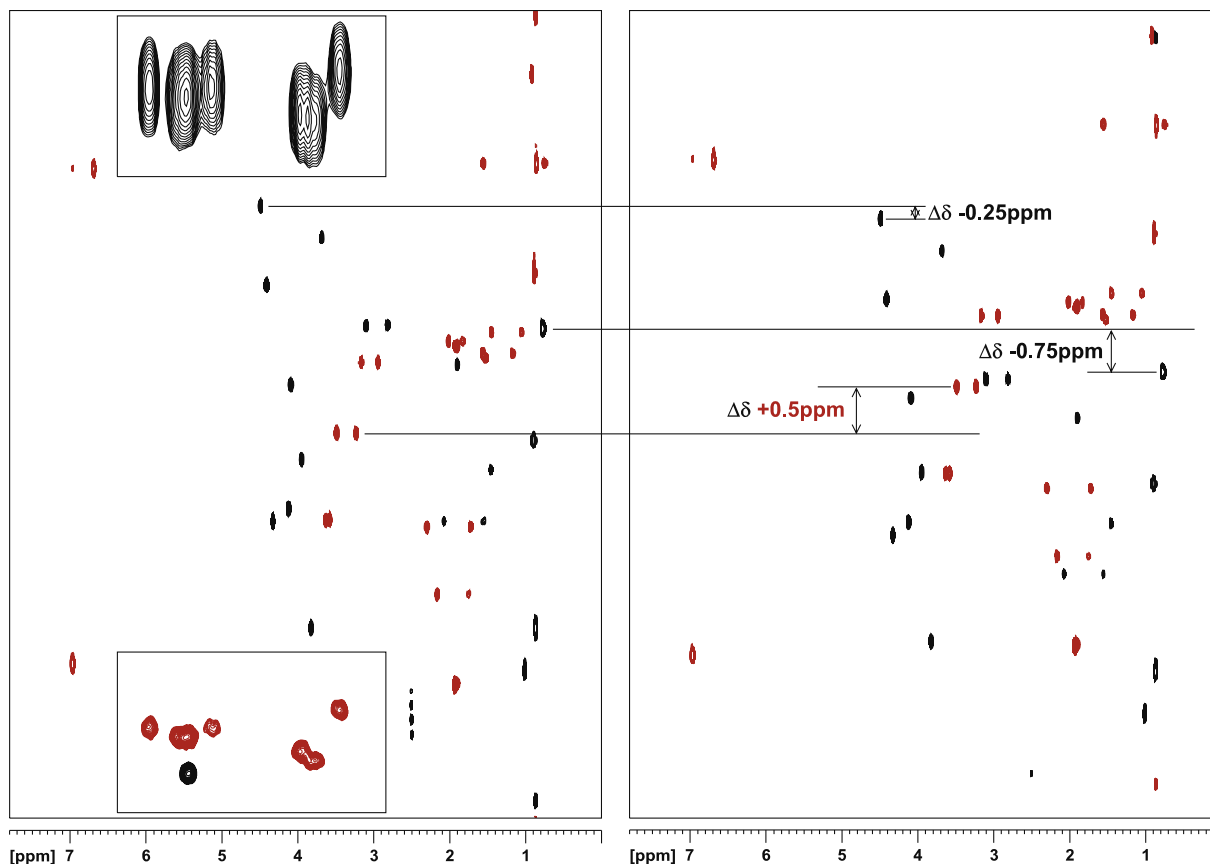
Fig. 9. 2D SHARC HSQC spectrum of Hymenistatin/DMSO-$d_6$ recorded utilizing the pulse sequence B (Fig. 5) with six regions of different width as determined from an overview spectrum. By running a second experiment with slightly modified carrier frequencies (±0.25 ppm, ±0.5 ppm and ±0.75 ppm) peaks are unambiguously assign to their respective regions. This is illustrated for three different regions. Black and red contours indicate positive and negative peaks. For space reasons the $^{13}C$ axes are omitted. The upper insert shows a selected part of a normal HSQC (the same as in Fig. 8), whereas the lower one shows the same part of the SHARC HSQC of this figure.

The sum of the preceding arguments illustrates the advantage of using a very low resolution preparation experiment prior to the start the actual SHARC type experiments. Execution of this preparation experiment will quickly deliver information about the distribution of sample chemical shifts and blank frequency regions. Actually, these empty frequency regions do not contain any spectroscopic information and can therefore be excluded from the allocation of measurement time. Again, we must notice that the execution of the broad band preparation experiment does not have the objective to resolve any peak position or resonances. It is rather a question to search for empty frequency regions. Besides, such an experiment will not take much more than a minute to record.

In the spectra presented above the emphasis was on improving the resolution. Therefor all spectra were run with the same overall experimental time (plus 75 s for the overview spectrum to define the regions in the case of Fig. 9). Of course the SHARC approach can also be used to speed up the acquisition (or any compromise between resolution and speed). In that case factors of 3 (four regions of 25 ppm, but 2 experiments as used in Fig. 10) and 7 (calculated for the region of Fig. 9 shown in the

insert and already including the time required for the overview spectrum) can be achieved.

As indicated above signal intensity is reduced due to longitudinal relaxation during those blocks in which a given region is "passive", i.e. the spins are along the $z$-axis. For a given region the amount of reduction depends on the sum of the $t_1$(max) values for all the other regions plus a smaller contribution from the lengths of the selective pulses (usually between 1 and 3 ms per pulse) and the $T_1$ relaxation time for a spin in this region. Since the spectra shown were optimized for resolution and therefor have a much longer $t_1$(max) time, they illustrate a worst case scenario in which additional $T_2$ relaxation contributes. Nevertheless taking a single trace through the peak at 4.47 ppm $^1H$ and 53.8 ppm $^{13}C$ chemical shift (Hα of Ile 8) and measuring the $S/N$ the loss for the spectrum of Fig. 8 amounts to a factor of close to 5. Out of this a factor 1.5 can be attributed to differences in $t_1$(max) (by running the experiment just for the region containing the peak of interest). This leaves about a factor of 3 coming from $T_1$ relaxation.

Another interesting feature of SHARC acquisition protocol is its general frequency selective character. Routinely, chemists or biologists are often interested in special spectral
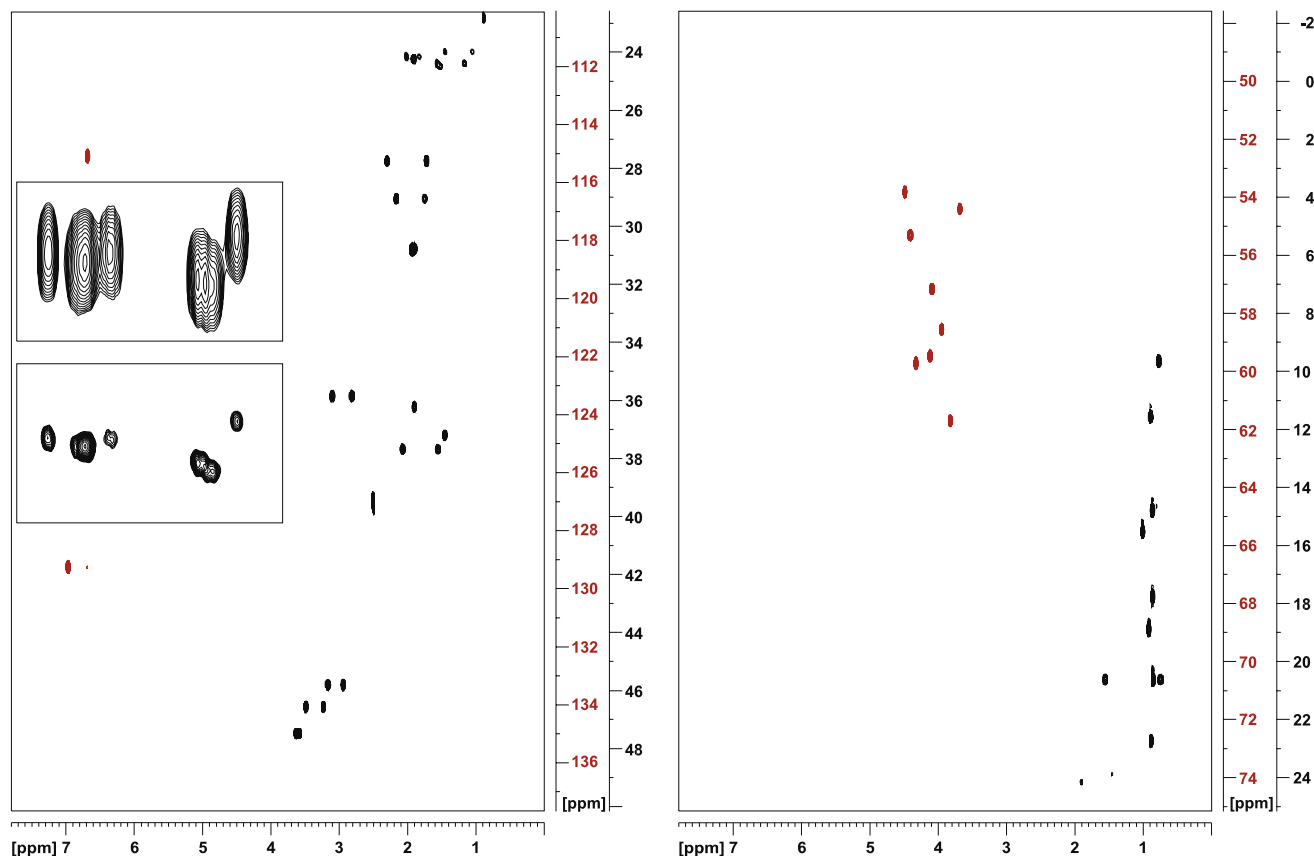
Fig. 10. 2D SHARC HSQC spectrum of Hymenistatin/DMSO-$d_6$ recorded utilizing the pulse sequence B (Fig. 5) with four regions of 25 ppm each. By running two experiments in an interleaved fashion and taking linear combinations between the two, the data is separated into two subspectra. The sign of the peaks differs for the two regions in each subspectrum. The figure shows multiple axes for the $^{13}C$ chemical shifts corresponding to the four regions. Black and red contours indicate positive and negative peaks. The color of the axes matches the color of the cross-peaks. The upper insert shows a selected part of a normal HSQC, whereas the lower one shows the same part of the SHARC HSQC of this figure.
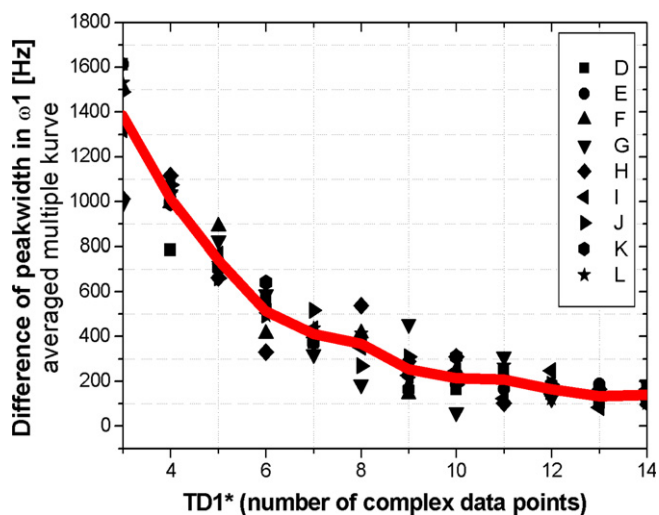


Fig. 11. The cross-peaks D–L were chosen randomly from a heteronuclear single quantum correlation (HSQC). The diagram shows the change of peak width difference in the $\omega_1$ dimension. The attenuation of the peak width difference is plotted as a function of increasing number of processed data points. The values were computed by a recursive subtraction of peak width from consecutive data points in $\omega_1$. The spectral bandwidth in the indirect dimension was 25 kHz.
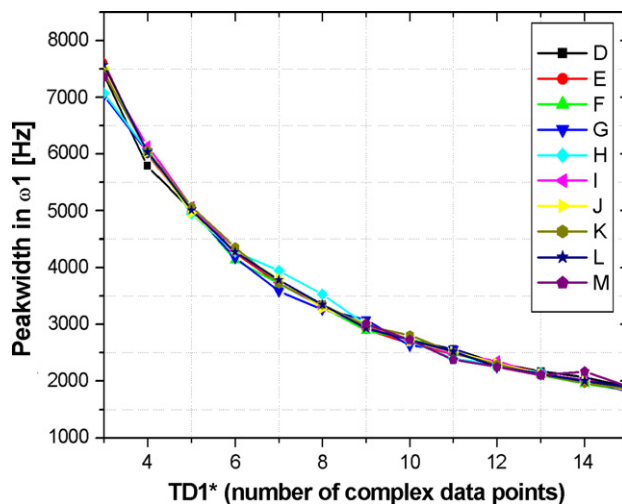


Fig. 12. The diagram shows the convergence of the line width improvement of arbitrary chosen cross-peaks D–M in $\omega_1$ obtained by gradually increasing the number of data points included in the processing scheme.

regions for monitoring of chemical reactions or in observing for transformations of various chemical functions. The corresponding bandselective NMR experiments—often

consisting of a wide band excitation step followed by application of frequency selective RF refocusing pulses and pulsed field gradients [52,53]—are usually done for a single region only. SHARC NMR in addition provides all other possible regions at the same time.

The fact that data manipulation according to a Hadamard matrix can be used to separate the data into different subspectra and the use of bandselective pulses, imply a certain proximity to Hadamard type methods [10–13]. There are though significant differences. Unlike to the method presented here, the "frequency labeling" in Hadamard type experiments is not done by incrementing a delay, but by a frequency selective pulse. Therefor the resolution in the indirect dimension directly correlates with the bandwidth of this pulse. Getting a high resolution would require to know all $^{13}C$ chemical shifts beforehand. Using bandselective pulses reduces the possible resolution or divides 2D spectra in subsets of an experiment of higher dimensionality [12,13]. There are also applications where bandselective pulses are modulated according to a Hadamard matrix in order to separate data into subsets, but still using conventional frequency labeling [54]. In this context, as well as in fast Hadamard type experiments in general, shaped pulses are used that are phase modulated for several frequencies at the same time (according to the number of required frequency bands). Each shaped pulse on its own has a given excitation profile, consisting of an excitation and a transition region. So when frequencies in a pulse modulated for multiple regions are getting too close together, the transition regions can overlap. This will lead to situations were flip angles are no longer properly defined. In SHARC NMR, this difficulty is bypassed, since only one region is excited at the time. So in case of overlap of transition regions peaks will simply show up in two different subspectra, but each time at their correct chemical shift. For both Hadamard and SHARC NMR an overlap of the excitation regions must not occur. Another advantage of SHARC NMR is the fact that the width of each region can be adjusted individually, which is not possible for the second type of using a Hadamard matrix for shaped pulses.

## 3. Conclusions

The SHARC principle provides a simplified approach to multidimensional NMR spectroscopy and takes new steps in the field of spectral aliasing. It provides new opportunities of non-uniformly assigning indirect domain spectral width to nuclear frequencies belonging to transverse magnetization rotating during the evolution period. Applied as described above, the SHARC method does not violate the Nyquist theorem, thus bypassing problems associated with this constraint. This is achieved by setting the respective carrier frequency at the center of the current indirect domain spectral width and utilizing the optimum size of $sw_1$. With the different schemes discussed above each peak can be unambiguously assigned to its region and thus to its

correct chemical shift. No back-calculation of chemical shift is required. With the SHARC method either the speed of an experiment can be increased. or the resolution of the resulting spectrum improved.

It can be expected that SHARC experiments will prove very useful for NMR investigations of structure and dynamics in natural product and protein samples.

Other homo- or heteronuclear correlation experiments based on the SHARC approach are also conceivable. Works along this line and other theoretical aspects of SHARC NMR are in progress.

## 4. Experimental

All experiments were acquired on a Bruker-Avance spectrometer (Bruker BioSpin, Rheinstetten, Germany) operating at 600.13 MHz proton frequency, equipped with a 5 mm triple resonance inverse probe and a $z$-axis pulsed field gradient accessory. All spectra were processed with the processing software TOPSPIN 2.0. The 2D data were collected on a sample of 20 mM Hymenistatin dissolved in pure DMSO-$d_6$ at a temperature $T = 303$ K.

For SHARC HSQC spectroscopy following pulse schemes were introduced: pulse sequence A (Fig. 4), pulse sequence B (Fig. 5) and pulse sequence C (Fig. 6). Thin filled rectangles represent non-selective 90° $^1H$ pulses, open wider rectangles are used for non-selective $^1H$ 180° pulses. The 90° $^{13}C$ selective Q5 pulses are shown as open Gaussian shapes. The length of the 90° $^{13}C$ selective Q5 Gaussian pulses was calculated on the basis of length × bandwidth = 6.586 for each region individually. Time reversed pulses are marked with T.R. The chirp pulses are defined in files in the Bruker library: Crp60,0.5,20.1 is a chirp pulse for inversion with a pulse length of 500 μs and is shown as open rectangle; Crp60comp.4 is a refocusing chirp pulse with a pulse length of 2 ms and is shown as open rectangles. The chirp pulses were defined with 1000 and 4000 points, respectively, a sweep width of 60 kHz and 20% smoothing. The power for the chirp pulses was adjusted to a level equivalent to a 90° rectangular pulse of 25.5 μs (9.8 kHz), which corresponds to a Q factor of 5 (determined with ShapeTool). Unless stated otherwise, pulses are applied along the $x$-axis. The filled sine shaped pulsed field gradients were 1 ms in length. The crusher pulsed field gradients are indicated as open sine envelopes and are 1 ms in length. The pulse field gradients are applied along the $z$-axis for selection or artifact suppression followed by a gradient recovery delay of 100 μs. Gradient strengths for the $zz$-filters of the pulse sequence B (Fig. 5): $G_1 = 41\%$, $G_2 = 17\%$, $G_3 = 50\%$, $G_4 = 31\%$, $G_5 = 11\%$, $G_6 = 35\%$, $G_7 = 9\%$, $G_8 = 5\%$, given as percentage of the absolute gradient strength of 53 G/cm.

The $^{13}C$ carrier frequency was changed at the points indicated by vertical arrows. The $^{13}C$ carrier frequency was jumped over a discrete set of values, each representing the on resonance frequency match of its corresponding indirect domain spectral width. The following delay

parameter was used: $\tau = (2 \times J_{HC})^{-1} = 3.45$ ms, initial value for $t_1$ increment $t_1(0) = 3$ μs. For pulse sequence B, regular States-TPPI phase cycling of $\varphi_3$ was used to obtain quadrature detection in the $^{13}$C ($F_1$) indirect dimension. GARP [55] $^{13}$C decoupling is applied at a field strength of $\gamma B_1/2\pi = 3.8$ kHz during the acquisition in $t_2$. The following phase cycling was used in the pulse sequences B (Fig. 5): $\varphi_3 = 0\,2$, $\varphi_4 = 0\,0\,2\,2$, $\varphi_{10} = 0\,0\,0\,0\,2\,2\,2\,2$ $\varphi_{rec} = 0\,2\,2\,0$. The calculation of incremental delays for the different spectral bandwidths was done at run time ("on the fly") according to the values of $\delta$, $\gamma$, and $\varepsilon$ constants based on the initial value of the spectral width in the indirect dimension. All HSQC spectra were recorded with 128 complex points in $F_1$ and 1024 in $F_2$ using 2 scans per increment and a 2 s delay between scans. The spectral bandwidth in $^1$H dimension was 11.02 ppm leading to an acquisition time of 154.88 ms. The regular HSQC spectrum used a sweep width of 161.62 ppm ($t_1$(max) of 5.25 ms). All SHARC HSQC spectra were acquired with sequence B (Fig. 5). For the spectrum in Fig. 8 a sweep width of 42 ppm ($t_1$(max) of 20.19 ms) with shaped pulses placed at 135, 95, 55 and 15 ppm was used. The spectra in Fig. 9 were recorded with 64 complex points in the indirect dimension each, so that the total number of points was again 128 complex points. The six regions had different widths with a maximum of 23.14 ppm and scaling factors for the increment of 1, 1.53, 2.67, 3.06, 1.48 and 1.66, respectively. The frequencies for the shaped 90° pulses were 123.23, 58.85, 47.53, 37.82, 26.66 and 12.26 ppm, respectively. For the spectra in Fig. 10 two interleaved experiments with 64 complex points each (total of 128 complex points) were performed. All regions had a sweep width of 25 ppm ($t_1$(max) of 15.36 ms) and frequencies of 125, 62.5, 38.5 and 12.5 ppm. The overview spectrum to define the regions was a gradient HMQC with 32 increments, one scan per increment and otherwise the same parameters as described above. Prior to 2D Fourier transformation, the data were linear predicted by a factor of two in the indirect dimension, apodized by multiplying with a 90°-shifted sine-squared function in both dimensions and then zero-filled to yield final matrices of 2048 ($F_1$) × 2048 ($F_2$) data points.

## Acknowledgments

## References

[1] J. Jeener, Ampere International Summer School II, Basko Polje, Yugoslavia, 1971.

[2] W.P. Aue, E. Bartholdi, R.R. Ernst, Two-dimensional spectroscopy. Application to nuclear magnetic resonance, J. Chem. Phys. 64 (1976) 2229–2246.

[3] R. Freeman, G.A. Morris, Two-dimensional Fourier transformation in NMR, Bull. Magn. Reson. 1 (1979) 5–26.

[4] T. Szyperski, G. Wider, J.H. Bushweller, K. Wüthrich, Reduced dimensionality in triple-resonance NMR experiments, J. Am. Chem. Soc. 115 (1993) 9307–9308.

[5] S. Kim, T. Szyperski, GFT NMR, a new approach to rapidly obtain precise high-dimensional NMR spectral information, J. Am. Chem. Soc. 125 (2003) 1385–1393.

[6] K. Ding, A. Gronenborn, Novel 2D triple-resonance NMR experiments for sequential resonance assignments of proteins, J. Magn. Reson. 156 (2002) 262–268.

[7] B.E. Coggins, R.A. Venters, P. Zhou, Filtered back projection for the reconstruction of a high-resolution (4,2)D CH3-NH NOESY spectrum on a 29 kDa protein, J. Am. Chem. Soc. 127 (2005) 11562–11563.

[8] E. Kupce, R. Freeman, Projection–reconstruction of three-dimensional NMR spectra, J. Am. Chem. Soc. 125 (2003) 13958–13959.

[9] E. Kupce, R. Freeman, Projection–reconstruction technique for speeding up multidimensional NMR spectroscopy, J. Am. Chem. Soc. 126 (2004) 6429–6440.

[10] E. Kupce, T. Nishida, R. Freeman, Hadamard NMR spectroscopy, Prog. NMR Spectrosc. 42 (2003) 95–122.

[11] E. Kupce, R. Freeman, Fast multi-dimensional Hadamard spectroscopy, J. Mag. Reson. 163 (2003) 56–63.

[12] B. Brutscher, Combined frequency- and time-domain NMR spectroscopy. Application to fast protein resonance assignment, J. Biomol. NMR 29 (2004) 57–64.

[13] P. Schanda, B. Brutscher, Hadamard frequency-encoded SOFAST-HMQC for ultrafast two-dimensional protein NMR, J. Magn. Reson. 178 (2006) 334–339.

[14] L. Frydman, T. Scherf, A. Lupulescu, The acquisition of multidimensional NMR spectra within a single scan, Proc. Natl. Acad. Sci. USA 29 (2002) 15858–15862.

[15] L. Frydman, A. Lupulescu, T. Scherf, Principles and features of single-scan two-dimensional NMR spectroscopy, J. Am. Chem. Soc. 125 (2003) 9204–9217.

[16] P. Pelupessy, Adiabatic single scan two-dimensional NMR spectroscopy, J. Am. Chem. Soc. 125 (2003) 12345–12350.

[17] D. Rovnyak, D.P. Frueh, M. Sastry, Z.Y. Sun, A.S. Stern, J.C. Hoch, G. Wagner, Accelerated acquisition of high resolution triple-resonance spectra using non-uniform sampling and maximum entropy reconstruction, J. Magn. Reson. 170 (2004) 15–21.

[18] V.Y. Orekhov, I. Ibraghimov, M. Billeter, Optimizing resolution in multidimensional NMR by three-way decomposition, J. Biomol. NMR 27 (2003) 165–173.

[19] Reviewed in: R. Freeman, E. Kupce, New methods for fast multidimensional NMR, J. Biomol. NMR 27 (2003) 101–114.

[20] P. Schanda, H. Van Melckebeke, B. Brutscher, Speeding up three-dimensional protein NMR experiments to a few minutes, J. Am. Chem. Soc. 128 (2006) 9042–9043 (and references cited therein).

[21] A. Ross, M. Salzmann, H. Senn, Fast-HMQC using Ernst angle pulses: an efficient tool for screening of ligand binding to target proteins, J. Biomol. NMR 10 (1997) 389–396.

[22] K. Pervushin, B. Vögeli, A. Eletsky, Longitudinal $^1$H relaxation optimization in TROSY NMR spectroscopy, J. Am. Chem. Soc. 124 (2002) 12898–12902.

[23] M.H. Levitt, P.K. Madhu, C.E. Hughes, Cogwheel phase cycling, J. Magn. Reson. 155 (2002) 300–306.

[24] N. Ivchenko, C.E. Hughes, M.H. Levitt, Application of Cogwheel phase cycling to sideband manipulation experiments in solid-state NMR, J. Magn. Reson. 164 (2003) 286–293.

[25] G. Zuckerstätter, N. Müller, Cogwheel phase cycling in common triple resonance NMR experiments for the liquid phase, J. Magn. Reson. 181 (2006) 244–253.

[26] R. Brüschweiler, F. Zhang, Covariance nuclear magnetic resonance spectroscopy, J. Chem. Phys. 120 (2004) 5253–5260.

[27] M. Sattler, M. Maurer, J. Schleucher, C. Griesinger, A Simultaneous, $^{15}N,^{1}H$- and $^{13}C,^{1}H$-HSQC with sensitivity enhancement and a heteronuclear gradient echo, J. Biomol. NMR 5 (1995) 97–102.

[28] OW. Sørensen, Aspects and prospects of multidimensional time-domain spectroscopy, J. Magn. Reson. 89 (1990) 210–216.

[29] E. Kupce, R. Freeman, B.K. John, Parallel acquisition of two-dimensional NMR spectra of several nuclear species, J. Am. Chem. Soc. 128 (2006) 9606–9607.

[30] A.J. Dunn, P. Sidebottom, Fast $^{1}H$–$^{13}C$ correlation data for use in automatic structure confirmation of small organic compounds, Mag. Reson. Chem. 43 (2005) 124–131.

[31] D. Jeannerat, High resolution in heteronuclear $^{1}H$–$^{13}C$ NMR experiments by optimizing spectral aliasing with one-dimensional carbon data, Magn. Reson. Chem. 41 (2003) 3–17.

[32] D. Jeannerat, D. Ronan, Y. Baudry, A. Pinto, J.P. Sauliner, S. Matile, NMR characterization of complex *p*-oligophenyl Scaffolds by means of aliasing techniques to obtain resolution-enhanced two-dimensional spectra, Helv. Chem. Acta 87 (2004) 2190–2207.

[33] R.R. Ernst, G. Bodenhausen, A. Wokaun, Principles of Nuclear Magnetic Resonance in One and Two Dimensions, Oxford Science Publications, Oxford, 1997.

[34] K. Takasugi (JEOL Ltd., Tokyo, Japan), 46th ENC Conference, (2005) Ultra-Fast Measurement in Multi-dimensional NMR: Spectrum Reconstruction from Folded Spectra with Multi-linear Sampling.

[35] I. Baskyr, T. Brand, M. Findeisen, S. Berger, Acquisition regime for high-resolution heteronuclear 2D NMR spectra, Angew. Chem. 118 (2006) 7985–7988.

[36] P. Sakhaii, (Sanofi-Aventis Deutschland GmbH) (2006) WO 2006/105909, (Verfahren zur Datenaufnahme Multidimensionaler NMR-Spektren durch Frequenzabhängige Faltung).

[37] G. Bodenhausen, D.J. Ruben, Natural abundance nitrogen-15 NMR by enhanced heteronuclear spectroscopy, Chem. Phys. Lett. 69 (1980) 185–188.

[38] M. Carravetta, M.H. Levitt, Long-lived nuclear spin states in high-field solution NMR, J. Am. Chem. Soc. 126 (2004) 6228–6229.

[39] R. Sarkar, P.R. Vasos, G. Bodenhausen, Singlet-state exchange NMR spectroscopy for the study of very slow dynamic processes, J. Am. Chem. Soc. 129 (2007) 328–334.

[40] T. Fujiwara, T. Anal, N. Kurihara, K. Nagayama, Frequency-switched composite pulses for decoupling carbon-13 spins over ultrabroad bandwidths, J. Magn. Reson. A 104 (1993) 103–105.

[41] T. Fujiwara, K. Nagayama, Optimized frequency/phase-modulated broadband inversion pulses, J. Magn. Reson. 86 (1990) 584–592.

[42] G. Bodenhausen, R.R. Ernst, The Accordion experiment, a simple approach to three-dimensional NMR spectroscopy, J. Magn. Reson. 45 (1981) 367–373.

[43] S. Hiller, F. Fiorito, K. Wüthrich, G. Wider, Automated projection spectroscopy (APSY), Proc. Natl. Acad. Sci. USA 120 (2005) 640–645.

[44] H.R. Eghbalnia, A. Bahrami, M. Tonelli, K. Halenga, J.L. Markley, High-resolution iterative frequency identification for NMR as a general strategy for multidimensional data collection, J. Am. Chem. Soc. 127 (2005) 12528–12536.

[45] F. Fiorito, S. Hiller, G. Wider, K. Wüthrich, Automated resonance assignment of proteins: 6D APSY-NMR, J. Biomol. NMR 35 (2006) 27–37.

[46] H. Post, D. Ratzel, P. Brunner, (Bruker Medizintechnik GmbH), (1982) DE 3209263 (Verfahren zum Messen der Magnetischen Kernresonanz).

[47] M.L. Kilfoil, P.T. Callaghan, Selective storage of magnetization in strongly relaxing spin systems, J. Magn. Reson. 150 (2001) 110–115.

[48] K.K. Kumashiro, K. Schmidt-Rohr, O.J. Murphy, K.L. Ouellette, W.A. Cramer, L.K. Thompson, A novel tool for probing membrane protein structure: solid-state NMR with proton spin diffusion and X-nucleus detection, J. Am. Chem. Soc. 120 (1998) 5043–5051.

[49] B.K. John, D. Plant, R.E. Hurd, Improved proton-detected heteronuclear correlation using gradient-enhanced Z and ZZ filters, J. Magn. Reson. A 101 (1993) 113–117.

[50] G. Otting, K. Wüthrich, Efficient purging scheme for proton-detected heteronuclear two-dimensional NMR, J. Magn. Reson. 76 (1988) 569–574.

[51] R. Freeman, S.P. Kempsell, M.H. Levitt, Broadband decoupling and scaling of heteronuclear spin–spin interactions in high-resolution NMR, J. Magn. Reson. 35 (1979) 447–450.

[52] C. Gailleta, C. Lequartb, P. Debeireb, J.M. Nuzillard, Band-selective HSQC and HMBC experiments using excitation sculpting and PFGSE, J. Magn. Reson. 139 (1999) 454–459.

[53] T.-L. Hwang, A.J. Shaka, Water suppression that works. Excitation sculpting using arbitrary wave-forms and pulsed-field gradients, J. Magn. Reson. A 112 (1995) 275–279.

[54] K. Krishnamurthy, Improved resolution using symmetrically shifted pulses, J. Magn. Reson. 153 (2001) 124–132.

[55] A.J. Shaka, P.B. Barker, R. Freeman, Computer-optimized decoupling scheme for wideband applications and low-level operation, J. Magn. Reson. 64 (1985) 547–552.

[56] F. Bloch, A. Siegert, Magnetic resonance for nonrotating fields, Phys. Rev. 57 (1940) 522–527.

[57] L. Emsley, G. Bodenhausen, Phase shifts induced by transient Bloch–Siegert effects in NMR, Chem. Phys. Lett. 168 (1990) 297–303.

[58] J. Boyd, N. Soffe, Selective excitation by pulse shaping combined with phase modulation, J. Magn. Reson. 85 (1989) 406–413.